

Singlet oxygen model evaluation of interstitial photodynamic therapy with 5-aminolevulinic acid for malignant brain tumor

Atsuki Izumoto
Takahiro Nishimura
Hisanao Hazama
Naokado Ikeda
Yoshinaga Kajimoto
Kunio Awazu

Singlet oxygen model evaluation of interstitial photodynamic therapy with 5-aminolevulinic acid for malignant brain tumor

Atsuki Izumoto,^{a,*} Takahiro Nishimura,^{a,*} Hisanao Hazama,^a
Naokado Ikeda,^b Yoshinaga Kajimoto,^b and Kunio Awazu^{a,c,d}

^aOsaka University, Graduate School of Engineering, Suita, Japan

^bOsaka Medical College, Department of Neurosurgery, Takatsuki, Japan

^cOsaka University, Graduate School of Frontier Biosciences, Suita, Japan

^dOsaka University, Global Center for Medical Engineering and Informatics, Suita, Japan

Abstract. Interstitial photodynamic therapy (iPDT) with 5-aminolevulinic acid (ALA) is a possible alternative treatment for malignant brain tumors. Further evaluation is, however, required before it can be clinically applied. Computational simulation of the photophysical process in ALA-iPDT can offer a quantitative tool for understanding treatment outcomes, which depend on various variables related to clinical treatment conditions. We propose a clinical simulation method of ALA-iPDT for malignant brain tumors using a singlet oxygen ($^1\text{O}_2$) model and $^1\text{O}_2$ threshold to induce cell death. In this method, the amount of $^1\text{O}_2$ generated is calculated using a photosensitizer photobleaching coefficient and $^1\text{O}_2$ quantum yield, which have been measured in several previous studies. Results of the simulation using clinical magnetic resonance imaging data show the need to specify the insertion positions of cylindrical light diffusers and the level of light fluence. Detailed analysis with a numerical brain tumor model demonstrates that ALA-iPDT treatment outcomes depend on combinations of photobleaching and threshold values. These results indicate that individual medical procedures, including pretreatment planning and treatment monitoring, will greatly benefit from simulation of ALA-iPDT outcomes. © The Authors. Published by SPIE under a Creative Commons Attribution 4.0 Unported License. Distribution or reproduction of this work in whole or in part requires full attribution of the original publication, including its DOI. [DOI: [10.1117/1.JBO.25.6.063803](https://doi.org/10.1117/1.JBO.25.6.063803)]

Keywords: photodynamic therapy; singlet oxygen; 5-aminolevulinic acid; protoporphyrin IX; singlet oxygen model.

Paper 190319SSR received Sep. 15, 2019; accepted for publication Nov. 26, 2019; published online Dec. 14, 2019.

1 Introduction

Photodynamic therapy (PDT), which involves light excitation of photosensitizers (PSs) to induce tissue destruction, has attracted attention as a potential alternative treatment for malignant brain tumors because of high tumor-to-normal (TN) tissue contrast, low photon energy, and minimal invasion.^{1,2} The treatment effectiveness of PDT has been demonstrated with Photofrin³, talaporfin sodium,^{4,5} and 5-aminolevulinic acid (ALA)-induced protoporphyrin IX (PpIX).^{6,7} ALA-induced PpIX is expected to have few side effects. Compared with other PSs, it has a higher TN uptake ratio^{6,8} and faster discharge from the body within 48 h.⁹ In addition, for deeply seated brain tumors, interstitial photodynamic therapy (iPDT) with ALA,^{10,11} which involves insertion of cylindrical light diffusers into tissues to efficiently direct photons to target regions, has been more effective in clinical studies compared with existing standard treatments.^{12,13} Several clinical studies have demonstrated that iPDT outcomes depend on the light dose, which is determined by the irradiation conditions, such as the number of inserted cylindrical light diffusers, their positions, the light fluence rate, and the irradiation time.¹³ The relationships between treatment outcomes and treatment conditions should be analyzed for safe and effective use of ALA

*Address all correspondence to Atsuki Izumoto, E-mail: izumoto-a@mb.see.eng.osaka-u.ac.jp; Takahiro Nishimura, E-mail: nishimura-t@see.eng.osaka-u.ac.jp

iPDT. Although further clinical studies might be able to provide these data, the collection of malignant brain tumor cases is difficult because these cancers are rare. In addition, many technical difficulties remain to be overcome in directly measuring the interaction of PSs and light *in vivo*.¹⁴

A computational approach that uses numerical models of treatment procedures can provide a prospective methodology to analyze iPDT outcomes for various combinations of parameters related to treatment conditions without experimental measurements. Recently, such an approach, which is called “*in silico* clinical trial” or “computational clinical trial,” has been applied for regulatory evaluation in the development of drugs and medical devices.^{15,16} In evaluation of ALA-iPDT treatment outcomes for brain tumors, the computational approach does not require the collection of target patients and overcomes the difficulties of direct measurement of treatment outcomes. For a computational clinical trial of ALA-iPDT, a photophysical model based on the mechanism of ALA-iPDT action should be constructed to estimate treatment outcomes.

In ALA-iPDT, the major cytotoxic species generated by light excitation of the PS is singlet oxygen ($^1\text{O}_2$).¹⁷ Such PDT is categorized as type II. For estimation of type II PDT outcomes, the amount of $^1\text{O}_2$ generated is a promising metric^{18–20} compared with other previously proposed metrics, including light dose^{21,22} and PDT dose.²³ Although direct measurement of $^1\text{O}_2$ by near-infrared spectroscopy has been proposed for PDT monitoring,²⁴ problems include a low signal-to-noise ratio and low spatial resolution, especially in iPDT. For the computational evaluation of iPDT outcomes, several studies have proposed $^1\text{O}_2$ generation calculation methods using various photokinetic and photochemical parameters, including reaction rate parameters and oxygen supply rate parameters.²⁵ Moreover, Zhu et al. proposed an empirical macroscopic $^1\text{O}_2$ model to calculate the spatiotemporal accumulation of reacted $^1\text{O}_2$.^{14,26} The parameters needed for the calculation were obtained from an *in-vivo* mouse experiment. However, for evaluation of human malignant brain tumor treatment, the various photokinetic and photochemical parameters for ALA-induced PpIX in human brain tissues need to be obtained.

In this study, to evaluate the ALA-iPDT outcomes *in silico*, we propose a method to calculate the accumulated concentration of the generated $^1\text{O}_2$ with a simple model using a photobleaching coefficient and a singlet oxygen quantum yield (SOQY). For the proposed method, the necessary parameters, photobleaching coefficient and SOQY for ALA-induced PpIX, were previously measured in several studies.^{27–32} To show the feasibility of the application using clinical data, ALA-iPDT outcomes were calculated using magnetic resonance imaging (MRI) data from a patient with malignant brain tumors. To understand the ALA-iPDT outcomes, the spatial distribution of generated $^1\text{O}_2$ and ALA-iPDT outcomes with respect to irradiation conditions were analyzed. The simulation can compensate for a lack of understanding of ALA-iPDT for effective treatment design and monitoring.

2 Theory and Method

2.1 Simulation Overview

The simulation procedure to estimate ALA-iPDT outcomes consists of three major calculations: insertion conditions for cylindrical light diffusers and calculation of spatial distribution of light fluence rate at positions (x, y, z) , $\varphi(x, y, z)$, calculation of spatial distribution of generated $^1\text{O}_2$ concentration, $D_{\text{SO}}(x, y, z)$, and estimation of cell death region, as shown in Fig. 1. A numerical three-dimensional (3-D) brain model with optical properties and PpIX concentrations was prepared. Cylindrical light diffusers were virtually inserted in the numerical 3-D brain model and the light propagation was calculated to obtain $\varphi(x, y, z)$. Using $\varphi(x, y, z)$, the $D_{\text{SO}}(x, y, z)$ was calculated. By setting the threshold of the generated $^1\text{O}_2$ concentration, $D_{\text{SO}(\text{th})}$, above the level at which cell death is induced, the treatment area in the numerical 3-D brain model was calculated. In this study, for quantitative comparison of several treatment conditions, treated volume (TV) and damaged volume (DV) values are defined as the volume of cell death region by $^1\text{O}_2$ in tumor tissues and normal tissues. Also, tumor coverage (TC) is defined as the ratio of TV to total tumor volume.

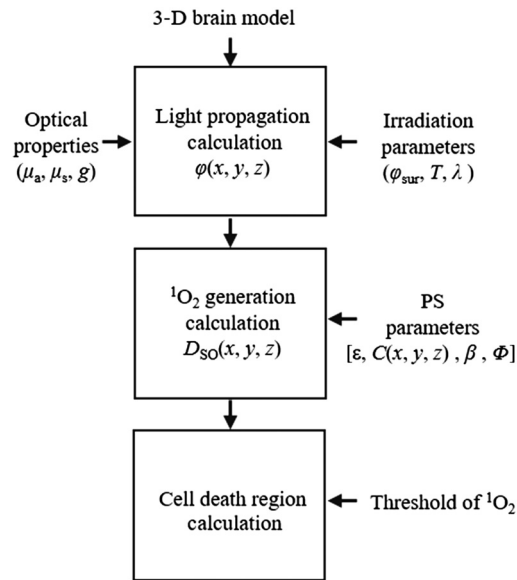


Fig. 1 Schematic diagram of the calculation of ALA-iPDT outcomes. Here, μ_a , μ_s , and g are the absorption coefficient, scattering coefficient, and anisotropy of scattering, respectively; $\varphi(x, y, z)$ is the spatial distribution of fluence rate at position (x, y, z) ; φ_{sur} , T , and λ are the light fluences on the surfaces of inserted diffusers, irradiation time, and wavelength of light, respectively; $D_{\text{SO}}(x, y, z)$ is the spatial distribution of generated $^1\text{O}_2$ at position (x, y, z) ; ε , $C(x, y, z)$, β , and Φ are the molar extinction coefficient, initial PS concentration at position (x, y, z) , photobleaching coefficient, and quantum yield for $^1\text{O}_2$ generation, respectively.

2.2 Numerical Tissue Model

To simulate ALA-iPDT outcomes, an anonymized MRI data set consisting of 156 two-dimensional slices (with resolution 512×512 pixels, pixel size $468 \mu\text{m}$, and slice thickness 1.25 mm) from a patient with a malignant brain tumor was used. The MRI slices were manually segmented into normal and tumor regions by a clinician using Synapse Vincent software (Fujifilm, Tokyo, Japan). The normal tissue regions around the tumor regions were assumed to be the white matter regions because most adult malignant brain tumors arise in white matter.³³ From the segmented MRI slices, a numerical 3-D voxel model having the segmented information was constructed³⁴ and optical property parameters were assigned to each voxel according to its tissue type. The absorption coefficient, μ_a (cm^{-1}), scattering coefficient, μ_s (cm^{-1}), and anisotropy factor of scattering, g , were set as 1.7 cm^{-1} , 365 cm^{-1} , and 0.9 , respectively, for the tumor regions and 0.7 cm^{-1} , 951 cm^{-1} , and 0.9 , respectively, for the white matter regions at the wavelength of 635 nm .³⁵ For iPDT outcome estimations, each voxel was divided into thirds in a direction perpendicular to the slice plane to give an isotropic voxel size of $468 \times 468 \times 417 \mu\text{m}^3$.

For detailed analysis of the influence of photobleaching and the initial PpIX concentration, a uniform brain tumor tissue model ($512 \times 512 \times 512$ pixels, $100 \times 100 \times 100 \mu\text{m}^3$), which consisted of tumor only, was used. Although PpIX is induced heterogeneously in tissues, the PpIX distributions were assumed to be uniform in the tumor region of the model for simplicity. The μ_a , μ_s , and g were set as 1.7 cm^{-1} , 365 cm^{-1} , and 0.9 , respectively, for the wavelength of 635 nm .³⁵ The photobleaching coefficient and initial PpIX concentration values were varied in evaluation.

2.3 Light Propagation Calculation

To obtain $\varphi(x, y, z)$ for the constructed numerical 3-D models, the Monte Carlo-based method, which is regarded as the gold standard to calculate light propagation in nonhomogeneous scattering media, such as biotissues, was used.³⁴ Here, the cylindrical fiber diffuser was assumed to have a radiation section that uniformly emits photons. The outer diameter was 1.1 mm and the

radiation length was 40 mm. To calculate light propagation from the inserted cylindrical light diffuser, a 3-D Monte Carlo program (mcxyz.c)³⁴ was customized. The launch points of photon packets were located inside the radiation section of the inserted cylindrical light diffuser according to Saccomandi et al.³⁶ As a laser source, a multiport laser system (ML 7710i, Modulight, Finland) with a wavelength of 635 nm and eight fiber ports was assumed.³⁷ Calculations of light propagation were performed for 1×10^7 photons. Irradiation time and irradiation power density were changed according to the simulation conditions.

2.4 Singlet Oxygen Generation Calculation

To calculate $D_{SO}(x, y, z)$, we adopted the SOQY model. PDT works well at oxygenation levels over 1% dissolved oxygen saturation rate (DO), but the effect decreases rapidly at lower levels of oxygenation.³⁸ The oxygen concentrations of tissues during PDT did not fall below 1% DO.³⁹ The SOQYs of ALA-induced PpIX in aqueous solutions have been reported and are very similar in 1% and 20% DOs, where the 1% and 20% DOs are calculated as 13 and 260 μM , respectively.³⁰ In the calculation, the same SOQY value were used for the normal and tumor regions.

Using the SOQY of PpIX, Φ , $D_{SO}(x, y, z)$ can be expressed as

$$D_{SO}(x, y, z) = \int_0^T f(x, y, z) \cdot C(x, y, z, t) \cdot \Phi dt, \quad (1)$$

where T is the irradiation time, $f(x, y, z)$ is the number of photons absorbed by PpIX in a unit time per unit concentration, and $C(x, y, z, t)$ is the PpIX concentration at position (x, y, z) at time t . From the calculated $\varphi(x, y, z)$, $D_{SO}(x, y, z)$ can be expressed as

$$D_{SO}(x, y, z) = \int_0^T \frac{1000 \cdot \varepsilon \cdot \ln(10) \cdot \varphi(x, y, z) \cdot \lambda}{hcN_A} \cdot C_0(x, y, z) \cdot \exp\left[-\frac{\varphi(x, y, z)}{\beta} t\right] \cdot \Phi dt \text{ [mM]}, \quad (2)$$

where ε is the molar extinction coefficient of PpIX, λ is the excitation light wavelength, h is Planck's constant, c is the speed of light, N_A is Avogadro's constant, $C_0(x, y, z)$ is the initial PpIX concentration at position (x, y, z) at time t , and β is the photobleaching coefficient. Fixed values of the parameters were $\varepsilon = 5000$ ($\text{cm}^{-1}\text{M}^{-1}$), $\lambda = 635$ (nm), $h = 6.626 \times 10^{-34}$ (Js), $c = 3.0 \times 10^{10}$ (cm/s), $N_A = 6.0 \times 10^{23}$ (mol^{-1}), and $\Phi = 0.77$.^{30,40} Other parameters were varied according to the evaluation items.

2.5 Cell Death Region Calculation

In the $^1\text{O}_2$ threshold models,^{26,41} cell death is induced at the region where $D_{SO}(x, y, z)$ exceeds $D_{SO(\text{th})}$. Normal tissues were assumed to be more resistant to $^1\text{O}_2$ toxicity than tumor tissues because of superoxide dismutase, which exerts an important protective function against oxygen toxicity.⁴² However, to avoid underestimation of $^1\text{O}_2$ toxicity in normal tissues, the $D_{SO(\text{th})}$ values for normal tissue damage were set to be equal to tumor tissue values. For estimation of the treatment region, the $D_{SO(\text{th})}$ value of 0.56 mM was used.²⁶

3 Results

3.1 Estimation of ALA-iPDT Outcomes Using Clinical Magnetic Resonance Imaging Data

To estimate the iPDT outcomes using clinical data, the TV and DV values were calculated with a cylindrical light diffuser inserted as shown in Fig. 2. Figure 2(a) shows the segmented tumor region and the insertion position. The total volume of the tumor region was 30.8 cm^3 . According to clinical studies,^{12,13} T and the light fluence at the surface of the diffuser, φ_{sur} , were set to 3600 s and 580 mW/cm^2 (linear density: 200 mW/cm), respectively. The $C_0(x, y, z)$ and

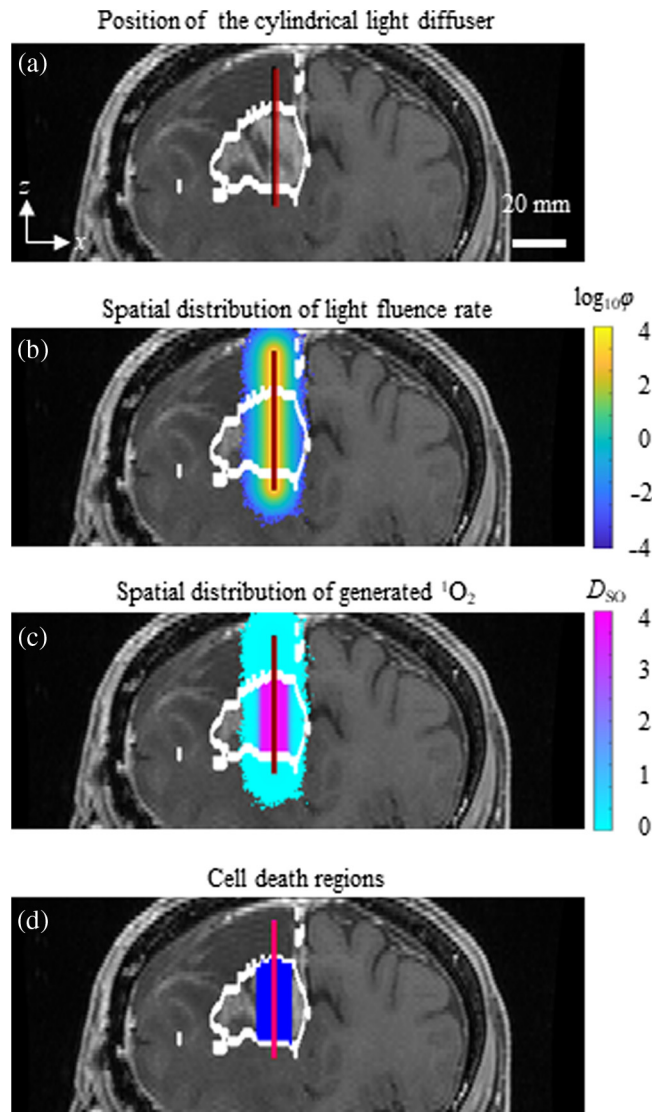


Fig. 2 Calculation of treatment region under a set of irradiation treatment conditions. (a) Tumor regions segmented by a clinician and insertion position of a cylindrical light diffuser. Tumor regions are demarcated with white lines and the surface of the cylindrical light diffuser is shown in red. (b) Spatial distribution of light fluence, $\varphi(x, y, z)$, calculated by a Monte Carlo-based algorithm, displayed as $\log_{10}[\varphi(x, y, z)]$ (mW/cm²). (c) Spatial distribution of generated ¹O₂, $D_{SO}(x, y, z)$ (mM), calculated from $\varphi(x, y, z)$. (d) Estimated treatment region (indicated in blue) setting an ¹O₂ concentration threshold to induce cell death at 0.56 mM.

$D_{SO(th)}$ were set to 5.8 μ M and 0.56 mM, respectively.^{26,43} Figures 2(b)–2(d) show the $\varphi(x, y, z)$ calculated by the Monte Carlo-based method, the $D_{SO}(x, y, z)$ calculated by inputting the calculated $\varphi(x, y, z)$, and the treatment region where $D_{SO}(x, y, z)$ exceeds $D_{SO(th)}$. TV and DV were calculated as 2.48 and 0 cm³, respectively. No damaged tissue in the normal tissue region was found under these irradiation conditions. When the PpIX uptake ratio of the tumor tissue region to white matter tissue (TN ratio) was 95,⁷ the DV was 0 cm³ even when the initial PpIX concentration in the tumor region was the reported maximum value⁴³ (28.2 μ M). This result is consistent with a previous clinical study that showed almost no damage to white matter in ALA-PDT.⁷ However, when the TN ratio was set to 12, the value of the brain tissue adjacent to the tumor,⁷ damage in the white matter region occurred at higher PpIX initial concentrations (>10.6 μ M) in the tumor region. This result shows that damage to normal tissue adjacent to the tumor is possible in clinical application.

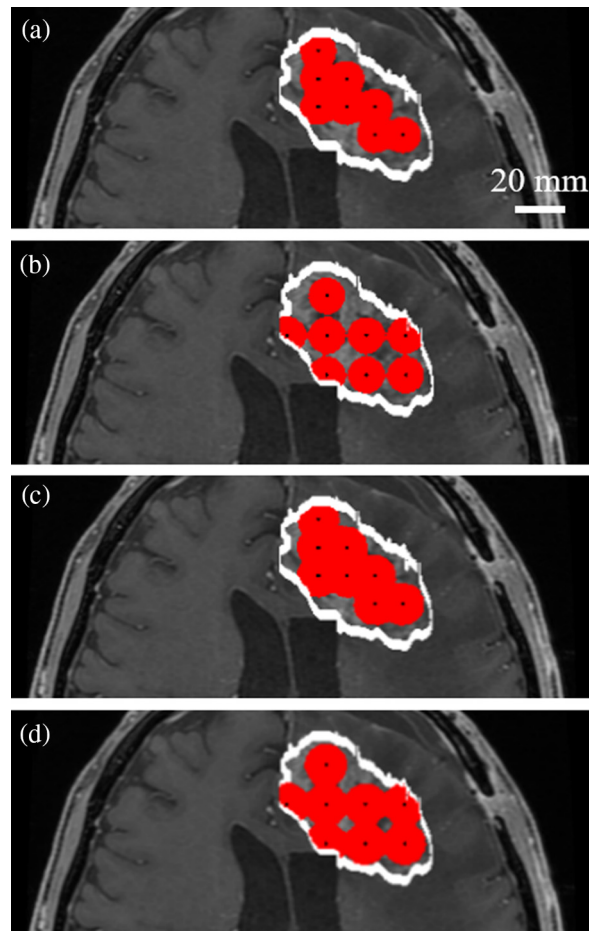


Fig. 3 Estimated treatment regions with eight cylindrical light diffusers with $D_{SO(th)}$ set to 0.56 mM. The tumor region is inside the white line. The treatment region is shown in red and the centers of the inserted fibers are indicated by black points. [Interdiffuser distance (cm), fluence rate at the diffuser surface (mW/cm^2)] = (a) (0.9, 580), (b) (1.25, 580), (c) (0.9, 2320), and (d) (1.25, 2320).

3.2 Evaluation of Irradiation Conditions

In ALA-iPDT, multiple cylindrical light diffusers are inserted depending on the tumor geometry.¹² To evaluate the dependence of the ALA-iPDT outcome on the insertion positions and φ_{sur} , TV and DV values were compared under several insertion conditions. The minimum distance between the diffusers (interfiber distance, L) has been determined as 0.9 cm to avoid a temperature increase above 42°C.¹² The distance L was, therefore, chosen as 0.9 cm to concentrate photons between the diffusers as much as possible. Figure 3(a) shows the treated regions when L , T , and Φ_{sur} were 0.9 cm, 1 h, and 580 mW/cm^2 (linear density: 200 mW/cm), respectively. TV and TC were calculated as 17.4 cm^3 and 0.56, respectively. The treated regions surrounding each diffuser overlapped. To improve the TC by avoiding region overlap, L was increased. However, TC was calculated as 0.55 when $L = 1.25$ cm [Fig. 3(b)]. Setting Φ_{sur} as 2320 mW/cm^2 (linear density: 800 mW/cm), the TCs were 0.66 when $L = 0.9$ cm [Fig. 3(c)] and 0.71 when $L = 1.25$ cm [Fig. 3(d)]. The iPDT outcomes are strongly dependent on the relationship between insertion positions and Φ_{sur} . These results demonstrate that both the insertion position and the Φ_{sur} should be designed by estimating the ALA-iPDT outcomes before treatment.

The relationships between generated $^1\text{O}_2$ concentration, D_{SO} , and light fluence were investigated. As shown in Fig. 4, D_{SO} reaches a maximal value with increasing light fluence because of photobleaching. This indicates that an increase in light fluence does not always improve the ALA-iPDT outcomes. Moreover, in the $^1\text{O}_2$ -based models, D_{SO} is required to merely exceed the $D_{SO(th)}$ value to provide treatment effects. When $D_{SO(th)}$ was 0.4, 0.56, and 0.72 mM,²⁶ the

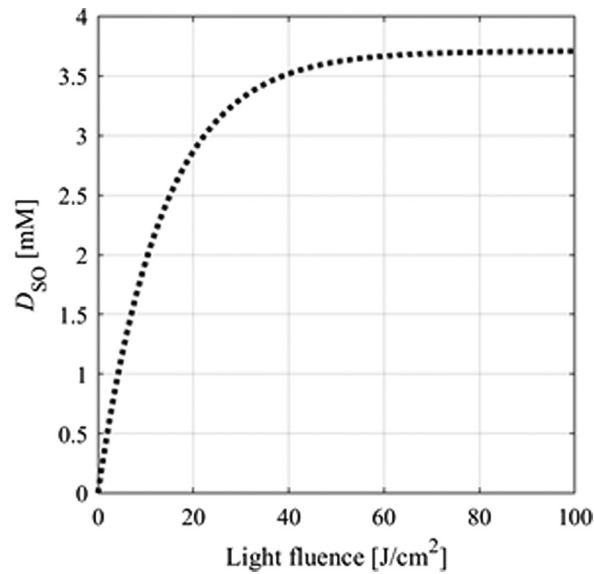


Fig. 4 Relationship between generated 1O_2 concentration, D_{SO} , and the light fluence for 0 to 100 J/cm².

required light fluences were 1.6, 2.3, and 3 J/cm², respectively. To avoid excessive irradiation, $D_{SO(th)}$ should be considered when determining light fluence.

3.3 Analysis of Photobleaching Influence

To evaluate the photobleaching effect, D_{SO} was compared between the proposed model with and without the photobleaching process. The parameters β , C_0 , which is PpIX initial concentration, T , and Φ_{sur} were 13.5 J/cm², 5.8 μ M, 3600 s, and 580 mW/cm², respectively. Figure 5 shows D_{SO} with and without photobleaching. When $D_{SO(th)}$ was assumed as 7.9 mM,²⁶ the D_{SO} exceeded the threshold only in the model without photobleaching. When $D_{SO(th)}$ was 0.4, 0.56, and 0.72 mM,²⁶ the D_{SO} exceeded the threshold to induce cell death in both models. Therefore, the parameter combinations of photobleaching and $D_{SO(th)}$ effect the iPDT outcomes. Next, using $C_0 = 5.8 \mu$ M, $T = 3,600$ s, $\Phi_{sur} = 580$ mW/cm², and $D_{SO(th)} = 0.56$ mM, TV was obtained to analyze the dependency of C_0 , as shown in Fig. 6. When β was 4.5, 13.5, and 33 J/cm²,²⁷⁻²⁹ the ALA-iPDT outcomes were induced when each C_0 was more than 0.4, 0.9, and 2.7 μ M. In the model without photobleaching, cell death was induced regardless of C_0 . As β becomes smaller, more C_0 is necessary for treatment. The optical properties of malignant brain tumor vary from patient to patient.³⁵ To estimate the possible ranges of the iPDT outcomes, TVs were calculated with the tissue optical properties, which maximized and minimized the light penetration depths. The maximum and minimum light penetration depths were defined using the standard deviation of the tissue optical properties. TV at the maximum light penetration depth was 20.0 cm³ when the μ_a , μ_s , and g were set as 0.92 cm⁻¹, 113 cm⁻¹, and 0.9, respectively. TV at the minimum light penetration depth was 2.1 cm³ when the μ_a , μ_s , and g were set as 2.5 cm⁻¹, 617 cm⁻¹, and 0.9, respectively. The TV difference was found since the reported standard deviations of optical properties are large.³⁵ A detailed analysis of the optical properties of the brain normal and tumor tissues is expected to increase the precision of the iPDT outcome estimations.

3.4 Analysis of PS Parameter Sensitivities

The sensitivities of C_0 and β were evaluated using the uniform living tissue model with optical properties of malignant brain tumors. Figure 7(a) shows the D_{SO} when C_0 was varied, assuming β and $D_{SO(th)}$ were 13.5 J/cm² and 0.56 mM, respectively. When C_0 was above 13.8 μ M, 1 J/cm² light irradiation was enough to induce cell death. When C_0 was 6.32 to 13.8 μ M, more light irradiation was necessary for treatment. Figure 7(b) shows the relationship between D_{SO}

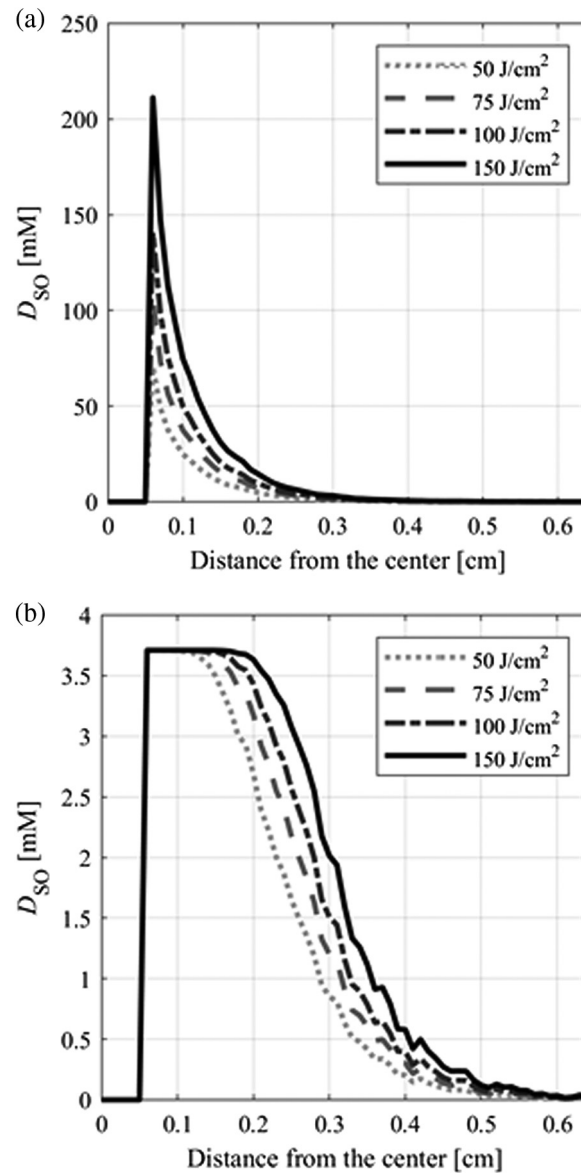


Fig. 5 Profiles of generated 1O_2 concentration, D_{SO} , from the center of the inserted diffuser for light fluence at the surface of the diffuser of 50, 75, 100, and 150 J/cm² (a) without and (b) with photobleaching when the coefficient was 13.5 J/cm².

and β when $C_0 = 5.8 \mu\text{M}$. The larger β led to higher D_{SO} because of a smaller decrease of C . When β was above 3.52 J/cm², 3 J/cm² light irradiation was enough for cell death. The D_{SO} varied depending on the light fluence and also on C_0 and β , which indicates that estimation of ALA-iPDT outcomes based only on light fluence, such as photon dose,^{21,22} is less accurate and that 1O_2 dose should also be considered.

4 Discussion

For the qualitative evaluation of ALA-iPDT outcomes, an estimation method based on the single oxygen model was proposed and assessed using MRI data. Compared with other single oxygen models, the number of required parameters was small and their values were previously reported and were available for calculation. According to the previous paper,³⁹ oxygen concentration was over 13 μM during PDT. The SOQY equals 0.77 in the concentration range.³⁰ However, in the other paper,¹⁸ the lowest oxygen concentration during PDT was about 1 μM . At the oxygen

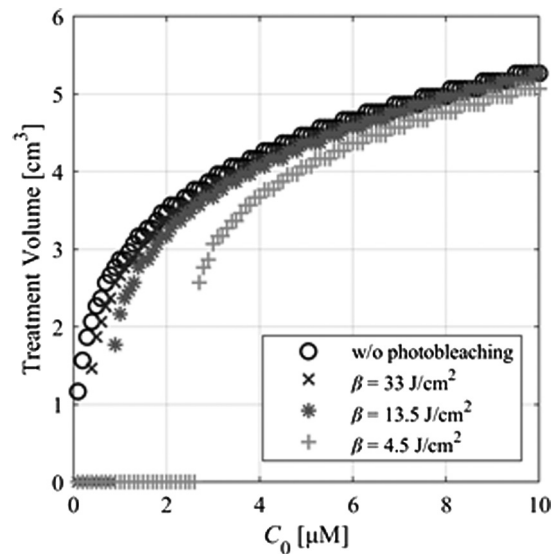


Fig. 6 Relationship between treatment volume and PpIX initial concentration, C_0 , of 0 to 10 μM in models with and without photobleaching for various values of photobleaching coefficients (4.5, 13.5, and 33 J/cm^2).

concentration, the SOQY is calculated as 0.63.³⁰ The SOQY is 18 % smaller compared to 0.77. It might affect the estimation accuracy of the ALA-iPDT. To prevent oxygen concentration decrease, oxygen supply control will offer a solution to keep the oxygen saturation in the brain tissues during PDT.¹² To confirm whether the proposed model can explain the ALA-iPDT outcomes, we compared the simulated results with those from previously reported animal experiments.⁷ In the estimated result shown in Fig. 2, even under severe light irradiation conditions, normal tissue damage was not induced when the TN ratio was set to 92.⁷ This supports the findings of Lilge and Wilson⁷ who demonstrated that there was no white matter damage at this TN ratio in animal experiments. In the simulation with the maximum accumulated PpIX concentration (28.2 μM ⁴³), normal tissue damage occurred with a TN ratio less than 32. Therefore, for ALA-iPDT treatment, irradiation conditions should be decided by considering C_0 and the TN ratio to prevent normal tissue damage.

To investigate the influence of irradiation conditions on ALA-iPDT outcomes, TCs were evaluated according to the L and Φ_{sur} values. As shown in Fig. 2, when Φ_{sur} was 580 mW/cm^2 (200 mW/cm^2), the TC when $L = 0.9$ cm was better than that when $L = 1.25$ cm. $L = 1.25$ was better for the Φ_{sur} of 2320 mW/cm^2 (800 mW/cm^2). These results indicate that consideration of the relationship between L and Φ_{sur} is required for pretreatment planning. The light fluence for effective treatment varied according to $D_{\text{SO(th)}}$. Precise $D_{\text{SO(th)}}$ will enable optimization of irradiation conditions and prevent excessive irradiation. $D_{\text{SO(th)}}$ can differ depending on tumor and PS types;²⁵ therefore, determination of $D_{\text{SO(th)}}$ in ALA-iPDT for malignant brain tumor is required.

Photobleaching is required in the $^1\text{O}_2$ model because photobleaching of ALA-induced PpIX has been observed in many studies.²⁷⁻²⁹ As shown in Fig. 6, when β of PpIX was 4.5, 13.5, or 33 J/cm^2 , cell death was induced when C_0 was more than 0.4, 0.9, and 2.7 μM , respectively. In the $^1\text{O}_2$ model without photobleaching, cell death was induced regardless of C_0 . In a clinical study of ALA-iPDT for malignant brain tumor⁴⁴ and in an *in-vivo* study of ALA-PDT,⁴³ an iPDT treatment effect was not confirmed when C_0 was 0.6 or below 1 μM , respectively. The estimated outcome was most consistent with the clinical and *in-vivo* results when $\beta = 13.5$ J/cm^2 . Parameters β and C_0 , however, have wide variations because of many factors, including solution conditions and individual differences.^{43,45} Previously reported β and C_0 values for PpIX have ranges from 1.8 to 33 J/cm^2 and from 0 to 28.2 μM , respectively.^{43,45} The difference in TV was 3.7 cm^3 between cases when β was 4.5 and 33 J/cm^2 ($C_0 = 5.8$ μM). Our simulated results show that the PS parameters β and C_0 have significant influence on the estimation results. For precise monitoring of ALA-iPDT outcomes during treatment, β and C_0 , which differ from

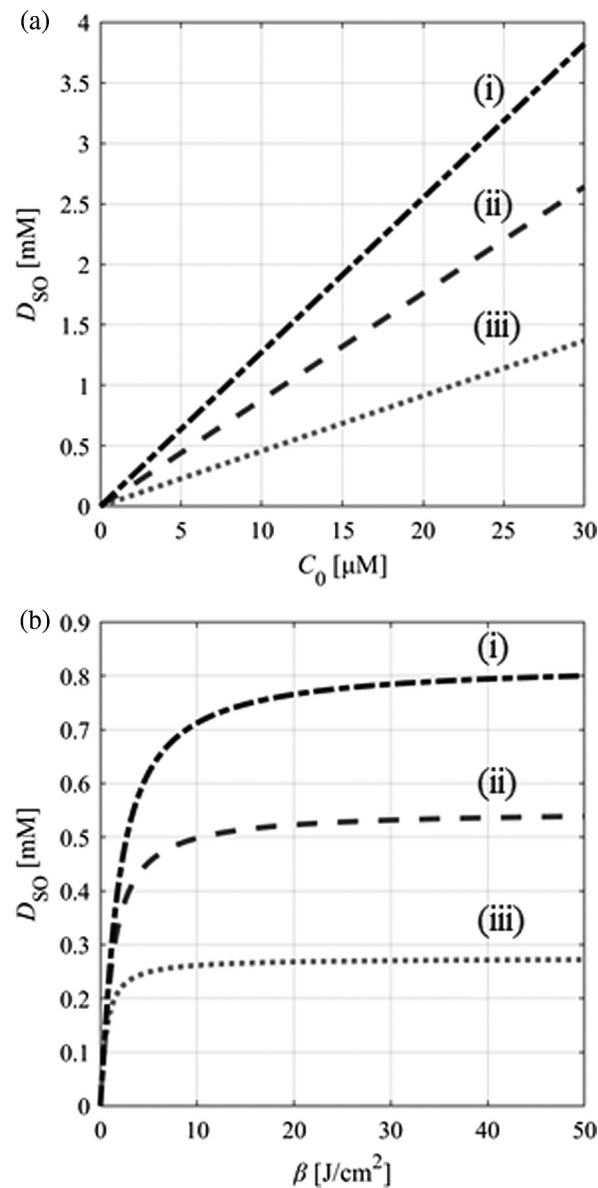


Fig. 7 Generated $^1\text{O}_2$ concentration, D_{SO} , versus (a) PpIX initial concentration, C_0 , from 0 to 30 μM ($\beta = 13.5 \text{ J}/\text{cm}^2$) and (b) photobleaching coefficient, β , of 0 to 50 J/cm^2 ($C_0 = 5.8 \mu\text{M}$). $^1\text{O}_2$ concentration threshold, $D_{SO(\text{th})}$, was 0.56 mM and light fluences were (i) 3 J/cm^2 , (ii) 2 J/cm^2 , and (iii) 1 J/cm^2 .

patient to patient, should be measured *in situ*, for example by a fiber optic measurement.⁴⁶ Use of the measured values leads to improvement of the estimation accuracy. However, since such parameter measurement before treatment is difficult, treatment planning will be performed by considering possible ranges of iPDT outcomes, which is derived from the reported parameter variances.^{43,45}

By comparing the reported clinical and animal studies, the proposed method can explain the ALA-iPDT outcomes using measured parameters. In the computational evaluation, combinations of treatment conditions that are difficult to quantify in clinical studies can be evaluated. Therefore, the outcome estimation method will provide prospective applications for ALA-iPDT development. For example, it is capable of helping treatment design before treatment and treatment monitoring during treatment at a low cost in various treatment conditions. In addition, it is useful for low-cost evaluation of treatment conditions for rare diseases with few cases compared to actual clinical trials. The $^1\text{O}_2$ model-based simulation can estimate the immediate outcomes

after light irradiation. The immune response has also been reported as a treatment factor in ALA-PDT.¹³ Incorporation of the immune response in the simulation will further refine the estimation of ALA-iPDT outcomes.

5 Conclusions

Treatment outcomes of ALA-PDT for malignant brain tumors depend on several parameters, including tumor tissue geometry, diffuser geometry, light irradiation-related variables, PS-related variables, and $^1\text{O}_2$ thresholds. In this study, to evaluate the ALA-PDT treatment conditions for malignant brain tumors, a treatment outcome estimation method was developed based on the mathematical model of $^1\text{O}_2$ generation using the SOQY and photobleaching coefficient. The estimated outcome results using measured parameters are consistent with previously reported clinical and animal ALA-PDT studies. Comparison between the proposed model with and without photobleaching shows that the light dose model is inadequate for the estimation of ALA-iPDT outcomes. These results indicate that pretreatment planning and treatment monitoring require accurate $D_{\text{SO(th)}}$, C_0 , and β values for the simulation of ALA-PDT outcome. The precise measurement of these values will improve the accuracy and provide better treatment design and outcomes. The simulation can estimate the immediate outcomes by $^1\text{O}_2$ after iPDT. The immune response is also considered as a treatment factor in ALA-PDT;⁴⁴ therefore, incorporation of the immune response in the simulation will improve iPDT outcomes.

Disclosures

The authors have no financial interests and no other potential conflicts of interest to disclose.

Acknowledgments

This work was supported by JSPS KAKENHI, Grant No. 19K12822.

References

1. D. Bechet et al., "Photodynamic therapy of malignant brain tumours: a complementary approach to conventional therapies," *Cancer Treat. Rev.* **40**, 229–241 (2014).
2. A. H. Kaye, G. Morstyn, and D. Brownbill, "Adjuvant high-dose photoradiation therapy in the treatment of cerebral glioma: a phase 1-2 study," *J. Neurosurg.* **67**, 500–505 (2009).
3. F. Jiang et al., "Photodynamic therapy with Photofrin reduces invasiveness of malignant human glioma cells," *Lasers Med. Sci.* **17**, 280–288 (2002).
4. Y. Muragaki et al., "Phase II clinical study on intraoperative photodynamic therapy with talaporfin sodium and semiconductor laser in patients with malignant brain tumors," *J. Neurosurg.* **119**, 845–852 (2013).
5. J. Akimoto, J. Haraoka, and K. Aizawa, "Preliminary clinical report on safety and efficacy of photodynamic therapy using talaporfin sodium for malignant gliomas," *Photodiagn. Photodyn. Ther.* **9**, 91–99 (2012).
6. J. Van Den Boogert et al., "5-Aminolaevulinic acid-induced protoporphyrin IX accumulation in tissues: pharmacokinetics after oral or intravenous administration," *J. Photochem. Photobiol. B Biol.* **44**, 29–38 (1998).
7. L. Lilge and B. C. Wilson, "Photodynamic therapy of intracranial tissues: a preclinical comparative study of four different photosensitizers," *J. Clin. Laser Med. Surg.* **16**, 81–91 (1998).
8. H. Hautmann et al., "In-vivo kinetics of inhaled 5-aminolevulinic acid-induced protoporphyrin IX fluorescence in bronchial tissue," *Respir. Res.* **8**, 33 (2007).
9. J. Webber, D. Kessel, and D. Fromm, "Side effects and photosensitization of human tissues after aminolevulinic acid," *J. Surg. Res.* **68**, 31–37 (1997).

10. P. J. Lou et al., "Interstitial photodynamic therapy as salvage treatment for recurrent head and neck cancer," *Br. J. Cancer* **91**, 441–446 (2004).
11. L. K. Lee et al., "Interstitial photodynamic therapy in the canine prostate," *Br. J. Urol.* **80**, 898–902 (2003).
12. T. J. Beck et al., "Interstitial photodynamic therapy of nonresectable malignant glioma recurrences using 5-aminolevulinic acid induced protoporphyrin IX," *Lasers Surg. Med.* **39**, 386–393 (2007).
13. A. Johansson et al., "Interstitial photodynamic therapy of brain tumors," *IEEE J. Sel. Top. Quantum Electron.* **16**, 841–853 (2010).
14. K. K. H. Wang et al., "Explicit dosimetry for photodynamic therapy: macroscopic singlet oxygen modeling," *J. Biophotonics* **3**, 304–318 (2010).
15. M. Viceconti, A. Henney, and E. Morley-Fletcher, "In silico clinical trials: how computer simulation will transform the biomedical industry," *Int. J. Clin. Trials* **3**, 37 (2016).
16. A. Carlier et al., "In silico clinical trials for pediatric orphan diseases," *Sci. Rep.* **8**, 1–9 (2018).
17. I. Coupienne et al., "5-ALA-PDT induces RIP3-dependent necrosis in glioblastoma," *Photochem. Photobiol. Sci.* **10**, 1868–1878 (2011).
18. T. Sheng et al., "Reactive oxygen species explicit dosimetry to predict local tumor control for Photofrin-mediated photodynamic therapy," *Proc SPIE.* **10860**, 108600V (2016).
19. G. Kareliotis, S. Liossi, and M. Makropoulou, "Assessment of singlet oxygen dosimetry concepts in photodynamic therapy through computational modeling," *Photodiagn. Photodyn. Ther.* **21**, 224–233 (2018).
20. H. Qiu et al., "Macroscopic singlet oxygen modeling for dosimetry of Photofrin-mediated photodynamic therapy: an in-vivo study," *J. Biomed. Opt.* **21**, 088002 (2018).
21. A.-A. Yassine et al., "Automatic interstitial photodynamic therapy planning via convex optimization," *Biomed. Opt. Express* **9**, 898 (2018).
22. S. R. H. Davidson et al., "Treatment planning and dose analysis for interstitial photodynamic therapy of prostate cancer," *Phys. Med. Biol.* **54**, 2293–2313 (2009).
23. M. S. Patterson, B. C. Wilson, and R. Graff, "In vivo tests of the concept of photodynamic threshold dose in normal rat liver photosensitized by aluminum chlorosulphonated phthalocyanine," *Photochem. Photobiol.* **51**, 343–349 (1990).
24. M. Niedre, M. S. Patterson, and B. C. Wilson, "Direct near-infrared luminescence detection of singlet oxygen generated by photodynamic therapy in cells in vitro and tissues in vivo," *Photochem. Photobiol.* **75**, 382–391 (2002).
25. M. G. Nichols and T. H. Foster, "Oxygen diffusion and reaction kinetics in the photodynamic therapy of multicell tumour spheroids," *Phys. Med. Biol.* **39**, 2161–2181 (1994).
26. T. C. Zhu et al., "In-vivo singlet oxygen threshold doses for PDT," *Photonics Lasers Med.* **4**, 59–71 (2015).
27. A. J. L. Jongen and H. J. Sterenborg, "Mathematical description of photobleaching in vivo describing the influence of tissue optics on measured fluorescence signals," *Phys. Med. Biol.* **42**, 1701–1716 (1997).
28. S. Iinuma et al., "In vivo fluence rate and fractionation effects on tumor response and photobleaching," *Cancer Res.* **59**, 6164–6170 (1999).
29. M. B. Ericson et al., "Photodynamic therapy of actinic keratosis at varying fluence rates: assessment of photobleaching, pain and primary clinical outcome," *Br. J. Dermatol.* **151**, 1204–1212 (2004).
30. T. Nishimura et al., "Determination and analysis of singlet oxygen quantum yields of talaporfin sodium, protoporphyrin IX, and lipidated protoporphyrin IX using near-infrared luminescence spectroscopy," *Lasers Med. Sci.* 1–15.
31. G. S. Cox, C. Bobillier, and D. G. Whitten, "Photooxidation and singlet oxygen sensitization by protoporphyrin IX and its photooxidation products," *Photochem. Photobiol.* **36**, 401–407 (1982).
32. A. A. Krasnovsky, "Photoluminescence of singlet oxygen in pigment solutions," *Photochem. Photobiol.* **29**, 29–36 (1979).
33. L. Lilge et al., "The sensitivity of normal brain and intracranially implanted VX2 tumour to interstitial photodynamic therapy," *Br. J. Cancer* **74**, 1691–1691 (1996).

34. S. L. Jacques, "Coupling 3D Monte Carlo light transport in optically heterogeneous tissues to photoacoustic signal generation," *Photoacoustics* **2**, 137–142 (2014).
35. N. Honda et al., "Determination of optical properties of human brain tumor tissues from 350 to 1000 nm to investigate the cause of false negatives in fluorescence-guided resection with 5-aminolevulinic acid," *J. Biomed. Opt.* **23**, 075006 (2018).
36. P. Saccomandi, E. Schena, and S. Silvestri, "Design of fiber optic applicators for laser interstitial thermotherapy: theoretical evaluation of thermal outcomes," in *Proc. Annu. Int. Conf. IEEE Eng. Med. Biol. Soc.*, pp. 3733–3736 (2013).
37. L. Orsila et al., "Photodynamic therapy platform for glioblastoma and intrabronchial tumors," *Proc. SPIE* **10480**, 1048007 (2018).
38. K. P. Nielsen et al., "Choice of optimal wavelength for PDT: the significance of oxygen depletion," *Photochem. Photobiol.* **81**, 1190 (2005).
39. T. C. Zhu, B. Liu, and R. Penjweini, "Study of tissue oxygen supply rate in a macroscopic photodynamic therapy singlet oxygen model," *J. Biomed. Opt.* **20**, 038001 (2015).
40. A. Kamkaew et al., "BODIPY dyes in photodynamic therapy," *Chem. Soc. Rev.* **42**(1), 77–88 (2013).
41. G. Karelitis et al., "Computational study of necrotic areas in rat liver tissue treated with photodynamic therapy," *J. Photochem. Photobiol. B Biol.* **192**, 40–48 (2019).
42. B. Popov et al., "Lipid peroxidation, superoxide dismutase and catalase activities in brain tumor tissues," *Arch. Physiol. Biochem.* **111**, 455–459 (2003).
43. A. Johansson et al., "5-aminolevulinic acid-induced protoporphyrin IX levels in tissue of human malignant brain tumors," *Photochem. Photobiol.* **86**, 1373–1378 (2010).
44. A. Johansson et al., "Protoporphyrin IX fluorescence and photobleaching during interstitial photodynamic therapy of malignant gliomas for early treatment prognosis," *Lasers Surg. Med.* **45**, 225–234 (2013).
45. R. M. Valentine et al., "Monte Carlo modeling of in vivo protoporphyrin IX fluorescence and singlet oxygen production during photodynamic therapy for patients presenting with superficial basal cell carcinomas," *J. Biomed. Opt.* **16**, 048002 (2011).
46. R. Penjweini et al., "Explicit dosimetry for 2-(1-hexyloxyethyl)-2-devinyl pyropheophorbide-a-mediated photodynamic therapy: macroscopic singlet oxygen modeling," *J. Biomed. Opt.* **20**, 128003 (2015).

Biographies of the authors are not available.